ADVANCED ENGINEERING MATERIALS

DOI: 10.1002/adem.201100356

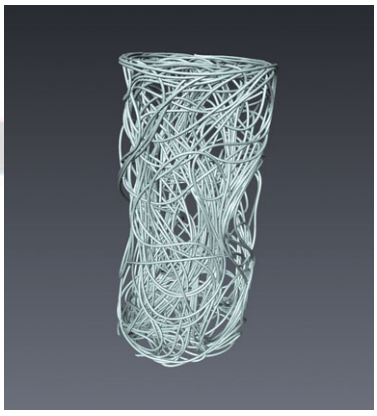

Mechanical Properties of Monofilament Entangled Materials

L. Courtois, E. Maire, M. Perez, D. Rodney, O. Bouaziz, Y. Brechet*

Monofilament entangled materials are a new type of materials with promising mechanical properties. They are made of a single wire randomly packed into a finite volume whose dimensions are much larger than the wire length, thus providing many self-contacts. Their complex internal architecture is investigated using X-ray tomography in order to link the microstructural evolution to the mechanical behaviour. This material exhibits very interesting properties in terms of vibration damping.

ADV. ENG. MATER. 2012, 00 . . . . . xx–xx

ADVANCED ENGINEERING MATERIALS

DOI: 10.1002/adem.201100356

Mechanical Properties of Monofilament Entangled Materials**

By *Loïc Courtois,* Eric Maire, Michel Perez, David Rodney, Olivier Bouaziz* and *Yves Brechet*

Monofilament entangled materials are a new type of materials with promising mechanical properties. They are made of a single wire randomly packed into a finite volume whose dimensions are much larger than the wire length, thus providing many self-contacts. Their complex internal architecture is investigated using X-ray tomography. The evolution of the number of contacts per unit volume, as well as of the density profiles, is monitored during a compression test in order to link the microstructural evolution of the sample to its mechanical behavior. This material exhibits very interesting properties in terms of vibration damping.

Playing with the architecture of a material is a promising way of tailoring its properties for multifunctional applications. What is now referred to as ''architectured materials'' (metal foams,[1] entangled materials,[2] steel wool,[3] etc.), has triggered numerous research in recent years, mostly for their ability to be engineered in order to exhibit specific combinations of properties, which ''classical materials'' could not offer. These materials have been proposed as ideal candidates for a top-down approach of ''materials by design.'' In this context, some studies have been carried out concerning entangled materials,[4] but only a few on monofilament entangled materials.[5–7] Such a material, with no filament ends, sliding contacts and a high relative porosity (80–95%), could exhibit interesting properties for shock absorption, vibration damping and ductility. The simplicity of the manufacturing process as well as the large permeability and the resistance to high and low temperatures, are also of interest for high technology applications, such as high strength seals or vibration damping materials.

Because of the complex architecture of these materials, X-ray tomography is used in this paper as a main characterization method. This technique enables a 3D nondestructive microstructural characterization of the material,[3] which can be coupled with an in situ mechanical characterization. Different parameters can be measured from the acquired 3D data (density profiles, number of contact per unit of volume, and volume fractions) and linked to the global mechanical behavior.

The purpose of this study is to investigate the compressive properties and the damping abilities of monofilament entangled materials for different wire diameters, volume fractions, and initial geometries of the wire.[8] Both the microstructural analysis and the mechanical analysis will provide information on the behavior of this architectured material.

1. Experimental Procedure and Results

1.1. Fabrication of the Steel Wire Entanglement

Steel wires were used in this study as a raw material. Their dimensions, as well as their mechanical properties are listed in Table 1.

The wire was first entangled manually to form a precursory wire-bundle. This bundle was then placed into a specific PTFE cylindrical die with a 15 mm diameter. The samples were initially 35 mm high with a 5% volume fraction. The control of

[*] *Dr. L. Courtois, Dr. E. Maire, Prof. M. Perez*
Université de Lyon, INSA de Lyon, MATEIS,
UMR CNRS 5510, 25 Avenue Jean Capelle,
69621 Villeurbanne, France
E-mail: loic.courtois@insa-lyon.fr
Prof. D. Rodney, Prof. Y. Brechet
SIMAP-GPM2, INPG, UMR CNRS 5266,
Domaine Universitaire BP 46 38402
Saint Martin d'Heres, France
E-mail: yves.brechet@simap.grenoble-inp.fr
Dr. O. Bouaziz
ArcelorMittal Research, Voie Romaine-BP30320,
57283 Maizières-lès-Metz Cedex, France
Centre des matériaux, Ecole des Mines de Paris,
UMR CNRS 7633 BP 87, 91003 Evry Cedex, France

[**] *The authors would like to thank the National Research Agency (MANSART, ANR-REG-071220-01-01) for funding this study. We thank Dr. J. Adrien for his help with the acquisition of the tomography scans. In addition, we would like to thank Dr. S. Meille and P. Clement for their help with the execution of the dynamic mechanical analysis.*

Table 1. Properties of the used wires.

Material	Diameters [μm]	Yield strength [MPa]
Stainless steel 304L	127, 200, and 280	200
Pearlitic steel	120	4000

the volume fraction was achieved through the measurement of the total length of the wire.

Once inside the mold, the samples were submitted to a constrained compressive test up to a final volume fraction of 17.5%. In this study, the compression state of the sample was characterized by its volume fraction, which appeared to be the most relevant parameter.

1.2. In situ X-ray Microtomography

In order to fully characterize the complex internal architecture of this material, an in situ compressive test was set up within the tomograph (Figure 1a). The cylindrical die, coupled to a piston rod, was placed inside a dedicated compressive machine, shown in Figure 1b,[9] which was fixed on the turntable of the tomograph.

The samples were compressed, step by step, and for each step, samples were unloaded. From the displacement of the grips and the initial length and diameter of the wires, it was possible to calculate the ''theoretical'' volume fraction of the sample during compression tests (starting at 5%). A 3D volume was acquired and reconstructed from a set of X-ray scans (Figure 1b). Each radiograph was acquired with a 24 μm voxel size.

1.3. Microstructural Characterization

In order to link the internal architecture to the global mechanical strength of the samples, a microstructural analysis was performed based on the 3D images. These were first processed to obtain a binary image where the wire appeared as white voxels, and the air as black. The homogeneity of the sample was studied by monitoring the evolution of the density distribution along the compression axis (*z*-axis). By measuring, for each cross-section of the sample (perpendicular to the *z*-direction), the ratio of the number of white pixels over the total number of pixels constitutive of the sample, we could measure a local density value, at a given *z* position (from top to bottom: 0–1). We could also measure the mean local orientation of the wire of the studied cross-section as a function of *z*. The aspect ratio of the cross-section of each intersection between the wire and the slice located at *z* provided information about the local orientation of the wire. Indeed, the cross-section of a perfectly vertical part of the wire appears as a circle whereas that of a segment perpendicular to the compression axis appears as a very elongated ellipse.

Figure 2 shows, for example, the evolution of the density and orientation distribution along the compression axis for a sample made of a stainless steel wire with a 200 μm diameter. We can notice a relatively homogeneous profile in the initial state (5%, figures on the left), except for the denser parts at the top and bottom of the sample (this ''wall effect'' will be discussed later in this paper). In terms of orientation, the internal part of the sample seems to be composed of wire sections oriented at an average angle of 35° whereas close to both ends, the wire tends to be oriented parallel to the horizontal faces of the mold.

With the increase of the volume fraction, densification peaks start to appear and grow (Figure 2d). From the orientation distribution along the compression axis (*z*-direction), we can clearly see that densification is accompanied by a reorientation of the wire in the direction perpendicular to the compression axis (highest angle between the *z*-axis and the wire). This structuring in the *z*-direction shows that the deformation of this material is not homogeneous and that localized deformation is accompanied by local densification and fiber reorientation.

To fully characterize the microstructure, it is also possible to study the density distribution along the radial direction. A local density was measured at a given *r* distance from the axis of the cylindrical die, averaged over the total height of the sample. By doing so for each position between the center (radial position = 0) and the side of the mold, a radial density

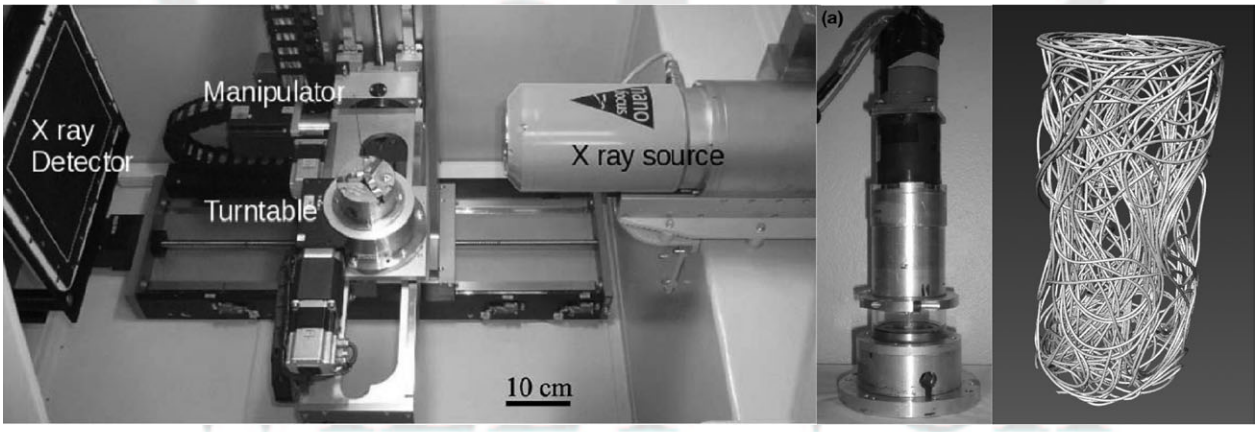

Fig. 1. (a) Internal chamber of the used tomograph, (b) in situ experimental compressive device, (c) example of a reconstructed 3D volume (diameter of the sample: 15 mm).

ADVANCED ENGINEERING MATERIALS **2012**,
DOI: 10.1002/adem.201100356

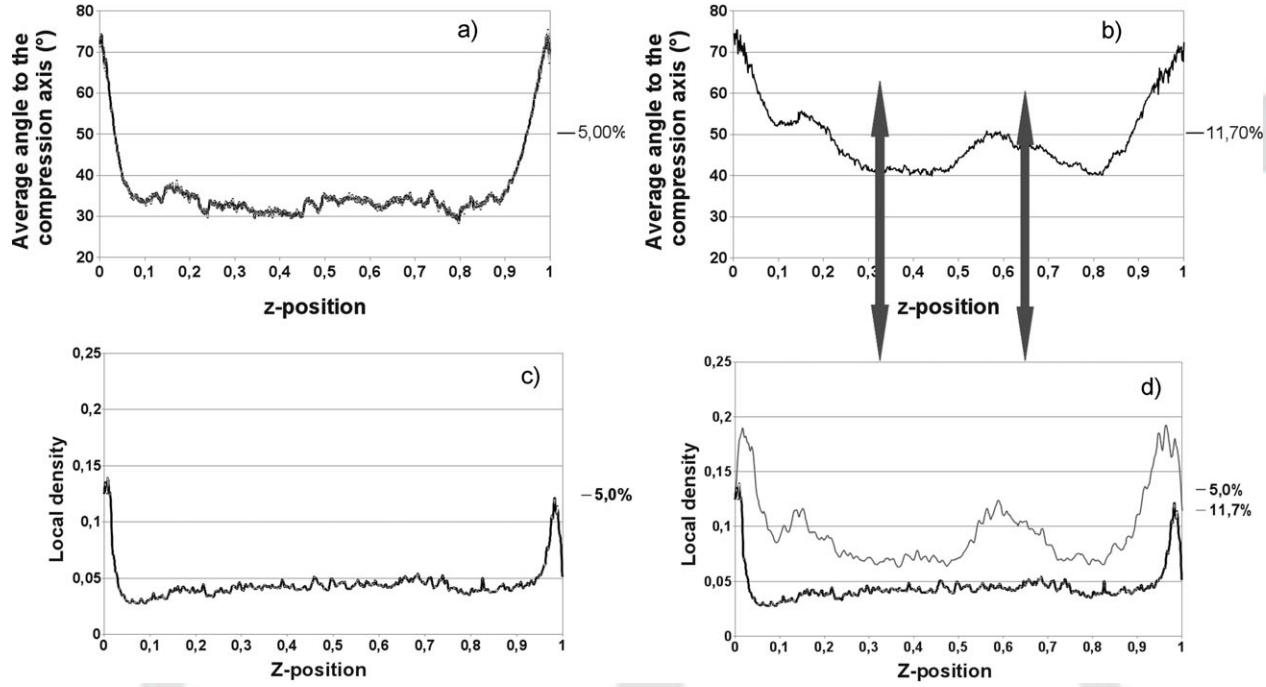

Fig. 2. (a–d) Evolution of the orientation (a and b) and local density (c and d) along the compression axis for two different densities (5%, figures a and c and 11.7% figures b and d).

profile could be measured. Figure 3a shows the influence of the diameter of the initial stainless steel wire used to produce the entanglement on the radial density profile. We can first notice a heterogeneous distribution of the wire with a higher local density close to the contact with the mold. This ''wall effect'' is typical of confined entangled media and seems to be less important for a smaller diameter of the wire. This was expected since a smaller wire diameter means a smaller bending modulus and thus more flexibility of the wire and easier arrangements for the same mold radius.

From the experiment with the pearlitic steel, we could study the influence of the yield strength of the wire on the density distribution. From the radial density profiles shown in Figure 3a, it can clearly be seen that the density gradient in case of high yield strength (pearlitic steel) is much more important than for low yield strength (stainless steel). This strong heterogeneity might also play a role on the mechanical response of this material. We have, locally, a very dense material which will tend to rigidify the structure.

Figure 3b presents the evolution of the normalized radial density profile (local density divided by the height of the sample) with the volume fraction, for a sample made of a 200 μm stainless steel wire. We can notice that the general shape of the profile does not evolve much. This would indicate that there is no re-arrangement of the wire in the radial direction when compressing the entanglement. The material is compressed along the compression axis with no evolution of the radial distribution.

From the binary 3D images, it was possible to measure the number of contacts per unit of volume. The data was first reduced to its center-line (skeletonization of the wire architecture). The whole structure then consisted in a list of segments and nodes where one contact corresponded to an H-like structure. By counting the number of segments shorter than the diameter of the wire (definition of a contact point), we

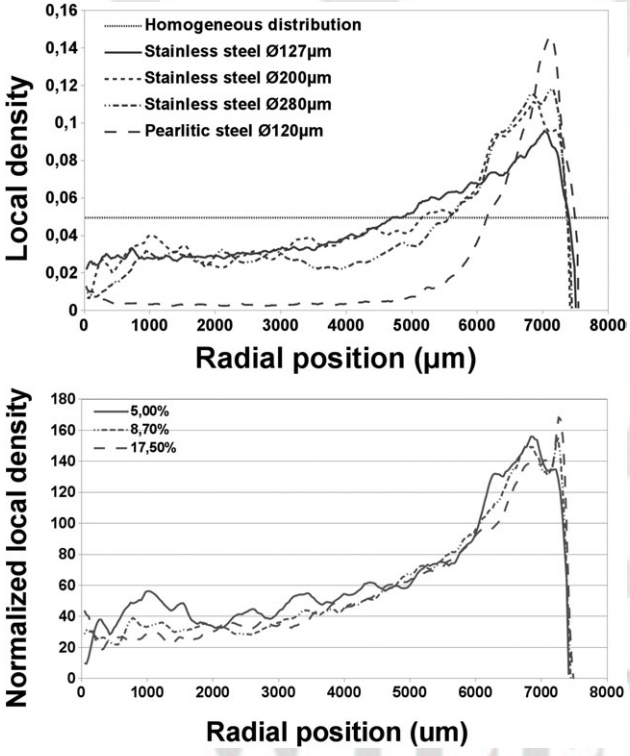

Fig. 3. (a) Influence of the diameter and yield strength on the radial density profiles. (b) Evolution of the radial density profile with the volume fraction.

could estimate the number of contacts per unit volume. This evaluation could be refined with the extra assumption that, if the distance between two short segments is smaller than the diameter of the wire, those two segments belong to the same contact point.

In this specific architectured structure, the mechanical strength mostly comes from the creation of contact points through the compression. Thus, from the tomography data, the evolution of the number of contacts per unit volume was studied. These experimental values can be compared to a model proposed by Toll which yields the following relationship between the number of contacts per unit of volume N_{cv} and the relative density ρ.[10]

$$N_{cv} = \frac{16f}{\pi^2 d_f^3}\rho^2 \quad (1)$$

where d_f is the diameter of the fiber and f is a parameter describing the fiber orientation distribution.

In the case of a sample made of a stainless steel wire, Figure 4 shows the evolution of the experimental and predicted number of contacts per unit volume with the volume fraction and wire diameter for the whole sample. We can see at first that, just as the model predicts, the number of contacts evolves as a function of the square of the volume fraction. Indeed, the slopes of the experimental results are almost identical to the one of the model in this log–log plot. This evolution tends to prove that the mechanical strength of this material will increase with the volume fraction. We can also notice that the contact density decreases with the diameter of the wire. This was expected since, for a smaller diameter, the length of the wire gets longer, for a given volume fraction. As a result, more contacts are created.

Although the general slope of the experimental plot does fit the model, the absolute values are not in agreement with the model. One reason might be that, since we are using the same resolution for all diameters, the contacts might not be as well defined for thin wires as for thicker ones. Additionally, some hypothesis of the model might not be fulfilled in the experiment. For example, the model assumes a random isotropic distribution of fiber orientations in an infinite system, whereas we have seen that there are strong heterogeneities near the walls and the fibers have a preferential orientation.

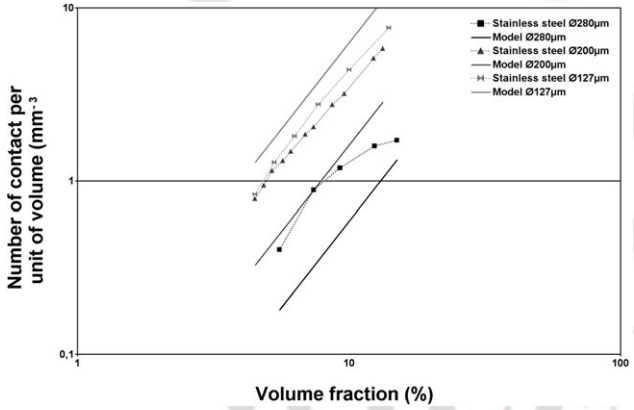

Fig. 4. Evolution of the number of contacts per unit of volume with the volume fraction.

From those measurements, it was possible to link the evolution of the internal microstructure to the mechanical behavior of this material and thus, have a better understanding of the behavior of the entangled media under compressive loading.

1.4. Mechanical Characterization

The samples were compressed with a strain rate of $5 \times 10^{-4}\,s^{-1}$. During the whole in situ compression test, a stress–strain curve was acquired. In this study, the stress values were plotted as a function of the volume fraction, which appeared to be more relevant for this type of entangled material.

For each compression step, corresponding to known volume fractions (6, 7, 8.7, 11.7, and 17.5%), the samples were unloaded and the strength of the entanglement was characterized by discharge modulus measurements (slope of the stress–strain curve at the first instant of the discharge). After unloading, the sample was reloaded in order to observe the hysteresis phenomenon.

As commonly observed in entangled materials,[11] the compressive mechanical behavior of the entanglement shows a nonlinear evolution (Figure 5a). There is no regime in which a purely linear elastic deformation could be observed. The material gets more and more dense as the number of contacts per unit volume increases, and the wire is deformed by bending between two contact points. We can also notice a very strong hysteresis phenomenon when a cyclic load is applied (unloading/reloading). This means that this material does indeed exhibit good damping abilities.

The stiffness of the material was assessed by measurements of the slope at the very first beginning of the unloading sequence (see Figure 5a). The stiffness of this material ranges from 20 to 200 MPa over the studied volume fraction range. Figure 5b shows that the entanglement tends to become stiffer as the volume fraction increases. We can also notice that, even though it was shown that for a smaller wire diameter, the contact density was higher, the samples tend to be less stiff. Therefore, there seems to be a compromise between the number of contacts per unit of volume and the wire stiffness, which decreases with the diameter. A higher yield strength of the wire seems (if the diameter is constant) to increase the rigidity of the sample. Indeed, the mechanical behavior of the sample made of a pearlitic wire is very close to the one made of a stainless steel wire with a diameter more than twice larger (Figure 5a), although the elastic moduli of the constitutive materials are very similar. This higher mechanical response for a higher yield strength might come from the very heterogenous density distribution that was previously shown but also from the higher mechanical properties of the wire itself. Furthermore, the deformation, in the case of the pearlitic

ADVANCED ENGINEERING MATERIALS 2012,
DOI: 10.1002/adem.201100356

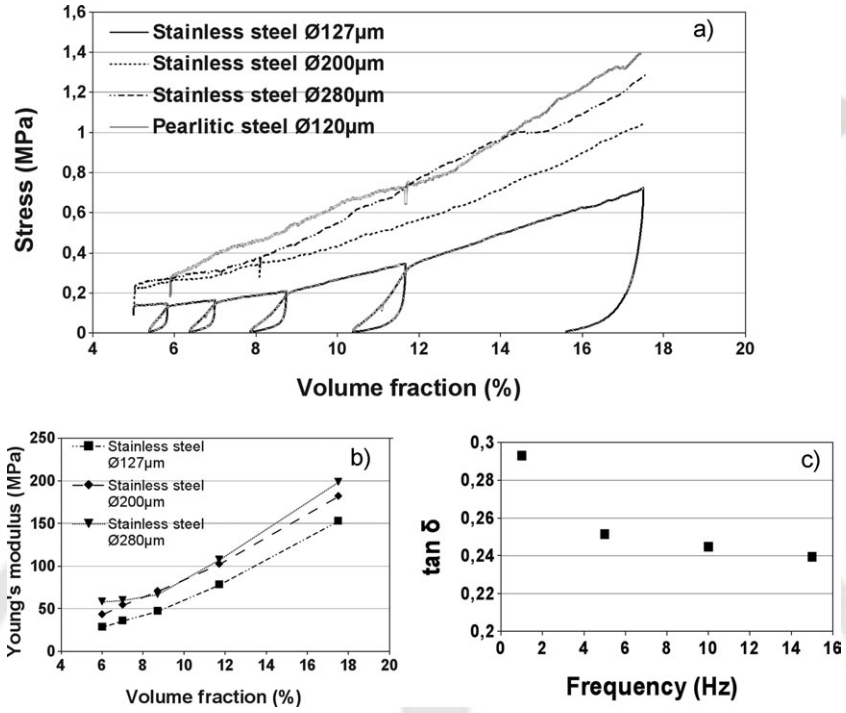

Fig. 5. (a) Stress = f(volume fraction), (b) evolution of the Young's modulus with the volume fraction, (c) evolution of the loss factor with the frequency for a 200 µm stainless steel wire.

steel wire, is almost entirely elastic whereas it is mostly plastic for stainless steel wires.

In parallel, a dynamic mechanical analysis was performed on a BOSE Electrofroce 3200. The samples were shaped inside the cylindrical PTFE mold and then taken out of it in order to place them in-between two compression plates. This procedure was selected to perform a measurement of the damping of the entanglement alone avoiding the effect of the mold. A sinusoidal displacement (0.3 mm amplitude) was imposed on a stainless steel sample (200 µm diameter) with a 10% volume fraction, submitted to a 5 N preload, and the resulting force was acquired. The phase angle difference (δ) between those two signals (force and displacement) was computed, from which the loss factor ($\tan\delta$) was deduced. This $\tan\delta$ value is an indicator of the capacity of the material to absorb energy. In this particular case, it is thought to be mostly through friction at contact points between wire segments.

Since the measurements were not constrained (no cylindrical die), only the stainless steel wire samples were analyzed. Indeed, the samples made of a pearlitic steel wire did not stay in shape when taken out of the containing mold.

This analysis was performed in order to estimate the loss factor of this material and to study the influence of the frequency on its ability to absorb energy. A mean $\tan\delta$ of 0.25 was observed, which is quite high if we consider that the one of polyurethane is around 0.5. Figure 5c) shows a decrease of the loss factor with the frequency. This would indicate that the energy dissipation mechanisms, mostly friction, are more efficient at low frequency.

2. Conclusion

The behavior of a steel entanglement was studied under a compressive load. Experiments were performed in situ with tomography and enabled a complete microstructural characterization of the very complex architecture of the material.

This monofilament entangled material was shown to be very heterogeneous with a very strong ''wall effect'' that could be reduced by using smaller wire diameters. The evolution of the number of contacts per unit of volume was studied and compared to a model for entangled media. The experiment showed an overall good agreement with the model. We were also able to relate the local orientation state to the density distribution inside the sample.

The stiffness of this material was shown to be in a 20–200 MPa range, which is relatively high for a highly porous entangled material. It is also worth noticing that the entangled structure, under a compressive load, exhibits a stiffness evolution, with the volume fraction, opposite to many usual cellular materials (foams, e.g., tend to get weaker when compressed). Its damping ability was also investigated and a dynamic mechanical analysis underlined its great capacity to absorb energy, with a loss factor of about 0.25.

Received: December 30, 2011
Final Version: June 18, 2012

[1] O. Caty, E. Maire, R. Bouchet, *Adv. Eng. Mater.* **2008**, *10*, 179.

[2] D. Rodney, M. Fivel, R. Dendievel, *Phys. Rev. Lett.* **2005**, *95*, 108004.
[3] J. P. Masse, L. Salvo, D. Rodney, Y. Brechet, O. Bouaziz, *Scr. Mater.* **2006**, *54*, 1379.
[4] C. Barbier, R. Dendievel, D. Rodney, *Comput. Mater. Sci.* **2009**, *45*, 593.
[5] P. Liu, G. He, L. Wu, *Mater. Sci. Eng. A* **2008**, *489*, 21.
[6] Q. Tan, P. Liu, C. C. Du, L. Wu, G. He, *Mater. Sci. Eng. A* **2009**, *527*, 38.
[7] P. Liu, G. He, L. Wu, *Mater. Sci. Eng. A* **2009**, *509*, 69.
[8] P. Liu, Q. Tan, L. WU, G. He, *Mater. Sci. Eng. A* **2010**, *527*, 3301.
[9] J. Y. Buffiere, E. Maire, J. Adrien, J. P. Masse, E. Boller, *Exp. Mech.* **2010**, *50*, 289.
[10] S. Toll, *Polym. Eng. Sci.* **1998**, *38*, 1337.
[11] D. Poquillon, B. Viguier, E. Andrieu, *J. Mater. Sci.* **2005**, *40*, 5963.

Q1: Author: Please check the suitability of the short title on the odd-numbered pages. It has been formatted to fit the journal's 45-character (including spaces) limit.

Q2: Author: Please check the title of the author Loïc Courtois.

*: Author: Please note that Figure for TOC will be printed in color.

ADVANCED ENGINEERING MATERIALS **2012**,
DOI: 10.1002/adem.201100356

WILEY-BLACKWELL

USING e-ANNOTATION TOOLS FOR ELECTRONIC PROOF CORRECTION

Required software to e-Annotate PDFs: Adobe Acrobat Professional or Adobe Reader (version 7.0 or above). (Note that this document uses screenshots from Adobe Reader X)
The latest version of Acrobat Reader can be downloaded for free at: http://get.adobe.com/uk/reader/

Once you have Acrobat Reader open on your computer, click on the Comment tab at the right of the toolbar:

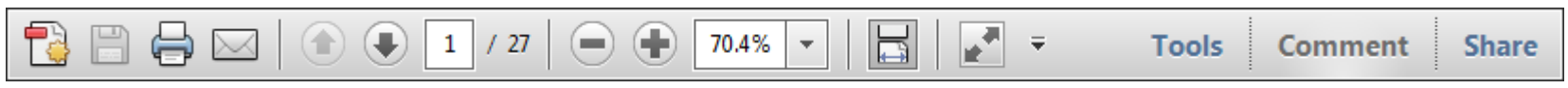

This will open up a panel down the right side of the document. The majority of tools you will use for annotating your proof will be in the Annotations section, pictured opposite. We've picked out some of these tools below:

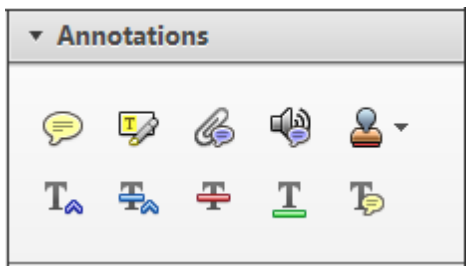

1. Replace (Ins) Tool – for replacing text.

Strikes a line through text and opens up a text box where replacement text can be entered.

How to use it

- Highlight a word or sentence.
- Click on the Replace (Ins) icon in the Annotations section.
- Type the replacement text into the blue box that appears.

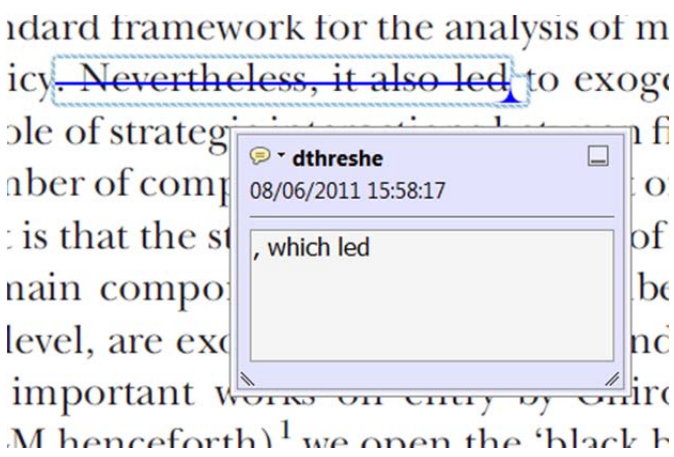

2. Strikethrough (Del) Tool – for deleting text.

Strikes a red line through text that is to be deleted.

How to use it

- Highlight a word or sentence.
- Click on the Strikethrough (Del) icon in the Annotations section.

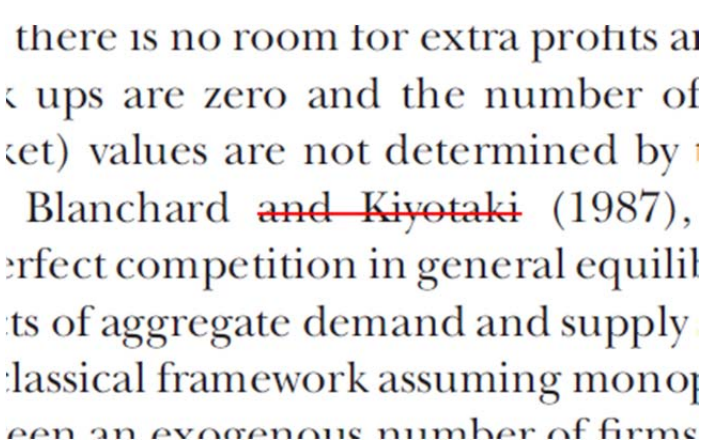

3. Add note to text Tool – for highlighting a section to be changed to bold or italic.

Highlights text in yellow and opens up a text box where comments can be entered.

How to use it

- Highlight the relevant section of text.
- Click on the Add note to text icon in the Annotations section.
- Type instruction on what should be changed regarding the text into the yellow box that appears.

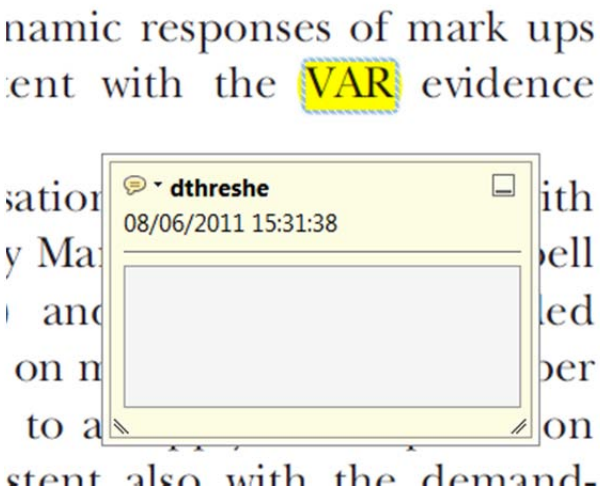

4. Add sticky note Tool – for making notes at specific points in the text.

Marks a point in the proof where a comment needs to be highlighted.

How to use it

- Click on the Add sticky note icon in the Annotations section.
- Click at the point in the proof where the comment should be inserted.
- Type the comment into the yellow box that appears.

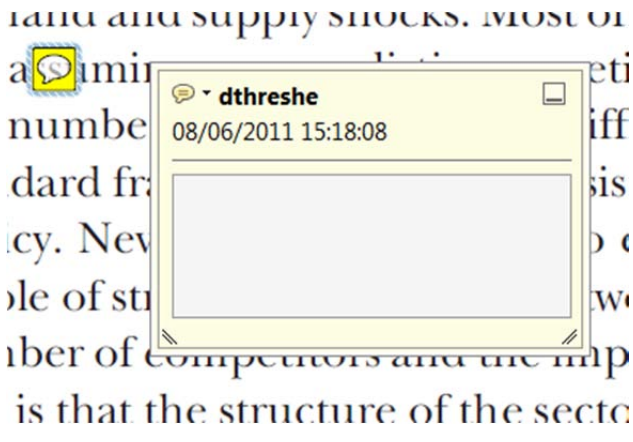

WILEY-BLACKWELL

USING e-ANNOTATION TOOLS FOR ELECTRONIC PROOF CORRECTION

5. Attach File Tool – for inserting large amounts of text or replacement figures.

Inserts an icon linking to the attached file in the appropriate pace in the text.

How to use it

- Click on the Attach File icon in the Annotations section.
- Click on the proof to where you'd like the attached file to be linked.
- Select the file to be attached from your computer or network.
- Select the colour and type of icon that will appear in the proof. Click OK.

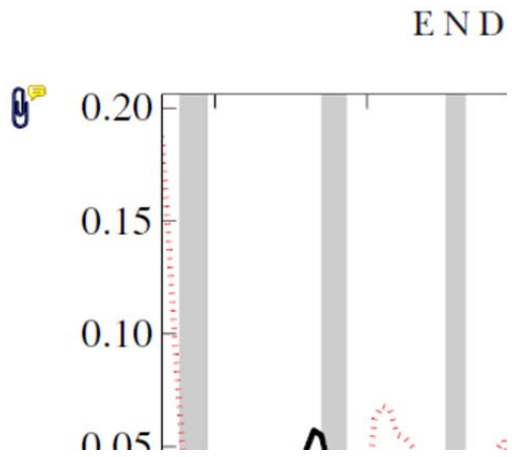

6. Add stamp Tool – for approving a proof if no corrections are required.

Inserts a selected stamp onto an appropriate place in the proof.

How to use it

- Click on the Add stamp icon in the Annotations section.
- Select the stamp you want to use. (The Approved stamp is usually available directly in the menu that appears).
- Click on the proof where you'd like the stamp to appear. (Where a proof is to be approved as it is, this would normally be on the first page).

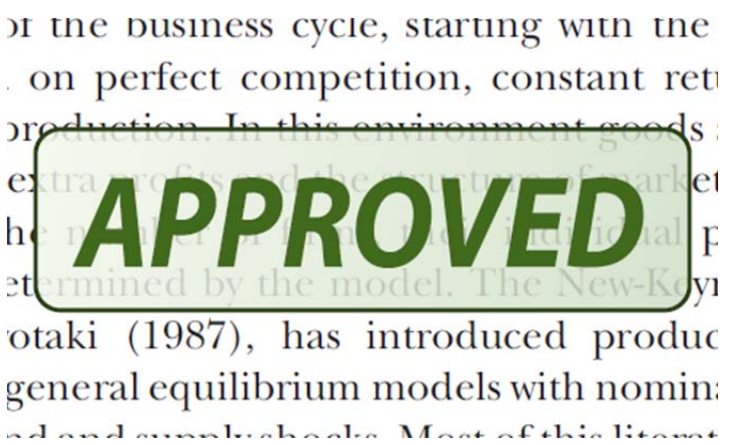

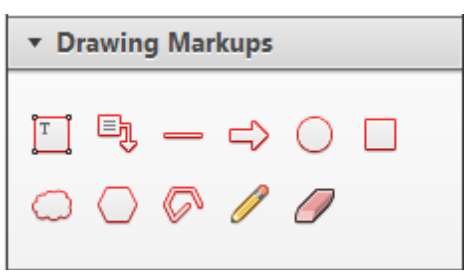

7. Drawing Markups Tools – for drawing shapes, lines and freeform annotations on proofs and commenting on these marks.

Allows shapes, lines and freeform annotations to be drawn on proofs and for comment to be made on these marks..

How to use it

- Click on one of the shapes in the Drawing Markups section.
- Click on the proof at the relevant point and draw the selected shape with the cursor.
- To add a comment to the drawn shape, move the cursor over the shape until an arrowhead appears.
- Double click on the shape and type any text in the red box that appears.

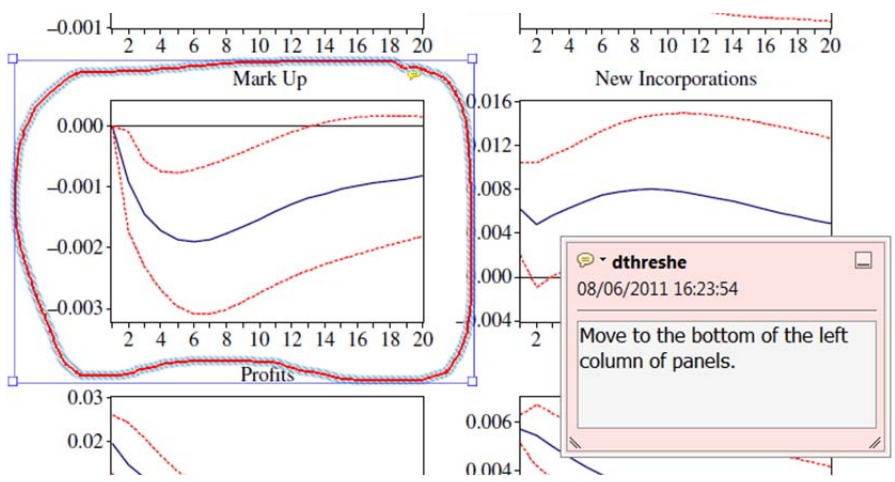

For further information on how to annotate proofs, click on the Help menu to reveal a list of further options:

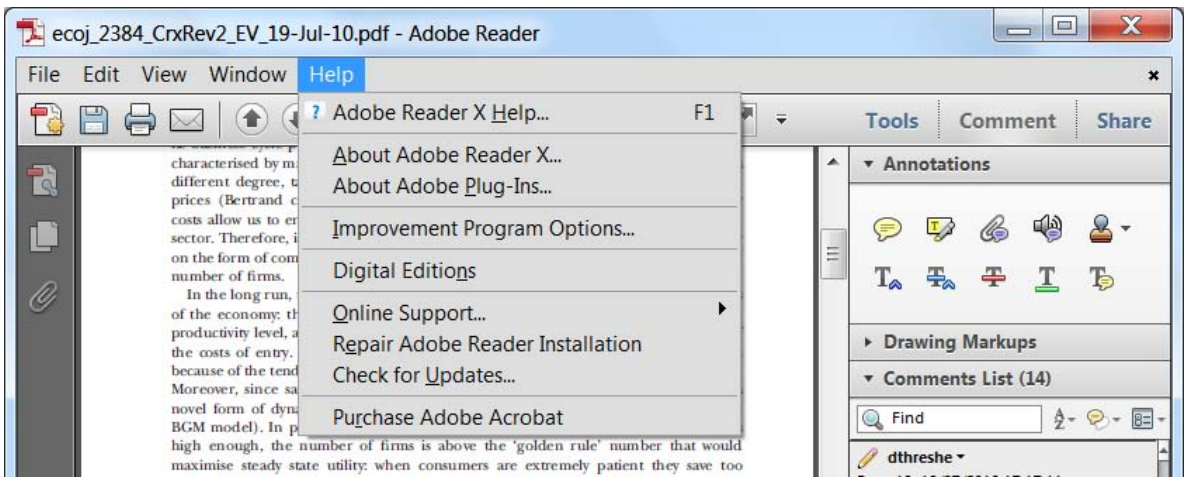

Advanced Engineering Materials

Reprint order form 2012
- please return with your proofs

Editorial office:
Wiley-VCH
Advanced Engineering Materials
Boschstrasse 12, 69469 Weinheim
Germany

Tel.: +49 (0) 6201 – 606 – 581 or 238
Fax: +49 (0) 6201 – 606 – 510

E-mail: aem@wiley-vch.de

http://www.aem-journal.com

Manuscript: adem._____

Author: _____

Please send me and bill me for

☐ no. of **reprints** via ☐ airmail (+ 25 Euro) ☐ surface mail

Please send me and bill me for

☐ no. of **copies of this issue** (1 copy: 20 Euro) via ☐ airmail (+ 25 Euro) ☐ surface mail

Please send me and bill me for

☐ **high-resolution PDF file** (330 Euro). My e-mail address:

_____

Please note: It is not permitted to present the PDF file in the internet or on company homepages

My VAT number is (institutes / companies in EU countries only):

_____

Invoices without VAT can only be processed with the VAT number of the institute / company. Please provide it with your order.

Purchase Order Number: _____

(Please contact your administrative office if you need one)

Mail reprints / copies of the issue to:

_____
_____
_____
_____
_____

Send bill to:

_____
_____
_____
_____
_____

Payment by credit card:

VISA ☐ MasterCard ☐ AMERICAN EXPRESS ☐

Card no. _ _ _ _ _ _ _ _ _ _ _ _ _ _ _ _

Expiry date: ___ / ___ **Security code:** _ _ _

Date, Signature:

Price list for reprints

Postage and handling charges included. All Wiley-VCH prices are exclusive of VAT.

No. of pages	Price (in Euro) for orders of					
	50 copies	100 copies	150 copies	200 copies	300 copies	500 copies
1-4	330	385	425	445	548	752
5-8	470	556	608	636	784	1077
9-12	610	717	786	824	1016	1396
13-16	744	874	958	1004	1237	1701
17-20	885	1040	1138	1196	1489	2022
for every additional 4 pages	140	164	175	188	231	315

WILEY-VCH